UC Davis

Title

Bioactive extracellular matrix scaffolds engineered with proangiogenic proteoglycan mimetics and loaded with endothelial progenitor cells promote neovascularization and diabetic wound healing

Permalink

Authors

He, Siqi
Walimbe, Tanaya
Chen, Hongyuan
et al.

Publication Date

DOI

Bioactive extracellular matrix scaffolds engineered with proangiogenic proteoglycan mimetics and loaded with endothelial progenitor cells promote neovascularization and diabetic wound healing

Siqi He [a,b], Tanaya Walimbe [c], Hongyuan Chen [b], Kewa Gao [a,b,e], Priyadarsini Kumar [b,e], Yifan Wei [b], Dake Hao [b,e], Ruiwu Liu [d], Diana L. Farmer [b,e], Kit S. Lam [d], Jianda Zhou [a], Alyssa Panitch [b,c], Aijun Wang [b,c,e,*]

[a] *Department of Burns and Plastic Surgery, The Third Xiangya Hospital of Central South University, China*
[b] *Department of Surgery, UC Davis, United States*
[c] *Department of Biomedical Engineering, UC Davis, United States*
[d] *Department of Biochemistry and Molecular Medicine, UC Davis, United States*
[e] *Institute for Pediatric Regenerative Medicine, Shriners Hospitals for Children Northern California, United States*

ABSTRACT

Diabetic ischemic wound treatment remains a critical clinical challenge. Neovascularization plays a significant role in wound healing during all stages of the tissue repair process. Strategies that enhance angiogenesis and neovascularization and improve ischemic pathology may promote the healing of poor wounds, particularly diabetic wounds in highly ischemic conditions. We previously identified a cyclic peptide LXW7 that specifically binds to integrin αvβ3 on endothelial progenitor cells (EPCs) and endothelial cells (ECs), activates vascular endothelial growth factor (VEGF) receptors, and promotes EC growth and maturation. In this study, we designed and synthesized a multi-functional pro-angiogenic molecule by grafting LXW7 and collagen-binding peptides (SILY) to a dermatan sulfate (DS) glycosaminoglycan backbone, named LXW7-DS-SILY, and further employed this multi-functional molecule to functionalize collagen-based extracellular matrix (ECM) scaffolds. We confirmed that LXW7-DS-SILY modification significantly promoted EPC attachment and growth on the ECM scaffolds *in vitro* and supported EPC survival *in vivo* in the ischemic environment. When applied in an established Zucker Diabetic Fatty (ZDF) rat ischemic skin flap model, LXW7-DS-SILY-functionalized ECM scaffolds loaded with EPCs significantly improved wound healing, enhanced neovascularization and modulated collagen fibrillogenesis in the ischemic environment. Altogether, this study provides a promising novel treatment to accelerate diabetic ischemic wound healing, thereby reducing limb amputation and mortality of diabetic patients.

1. Introduction

In 2019, the International Diabetes Federation (IDF) estimated a global population of 415 million people with diabetes mellitus, and that the number of people affected will increase to 700 million by 2045 [1]. IDF also estimated that 25% of this population will develop diabetic foot ulcers (DFU) in their lifetime [2], with over 65% of DFUs having an ischemic pathology prone to serious infections, leading to diabetes-related lower extremity amputations [3]. Moreover, ulcers and other foot complications contribute greatly to diabetes-related hospitalizations, and thus represent a significant healthcare burden. Accelerating the wound healing process in ischemic DFU would reduce the need for lower extremity amputation, improve survival of patients suffering from DFUs, and decrease diabetes-related hospitalizations.

The current standard of care for DFU treatment includes debridement of the wound, antibiotic management of any infection, ulcer off-loading, and revascularization surgeries, if indicated. The current bioengineered scaffold therapies using commercially available scaffolds such as Dermagraft

(human fibroblast-derived dermal substitute) and Regranex (recombinant PDGF, also known as becaplermin gel), or tissue engineered skin, but all have disadvantages due to multiple repeat applications for efficacy, secondary surgeries, delayed healing, and fibrosis [4]. Moreover, none of them are designed to improve re-vascularization specifically. To overcome these difficulties, stem cell-based therapy to improve revascularization of the wounds has emerged as a new approach for chronic wound healing [5]. Neovascularization plays a significant role in wound healing during all stages of the tissue repair process; therefore, a therapy that improves the vascularization of the damaged and regenerating tissue will hasten the healing process, leading to better outcomes [6].

Endothelial progenitor cells (EPCs) derived from bone marrow have the potential to differentiate into mature endothelial cells (ECs), leading to tissue vascularization [7]. Velazquez et al. [8] demonstrated that EPCs are present in much higher numbers in non-ischemic wounds compared to ischemic wounds generated in the same animal. In diabetic ischemic wounds, the lack of access to peripheral blood further dampens EPC migration to the wounds which leads to impaired healing due to poor oxygenation and nutrient and waste transport [9]. This lack of access to circulation and thus impaired endogenous EPC recruitment to the wound sites highlight the need for exogenous EPC delivery to the ischemic sites to effectively improve wound healing. Localized exogenous EPC delivery to the ischemic wound site with biological scaffolds that support EPC binding, survival, retention and engraftment will have a profound beneficial effect on wound healing in patients with ischemic wounds.

Porcine small intestinal submucosa (SIS) is an FDA-approved, commercially available, collagen-based natural extracellular matrix (ECM) scaffold that has been widely used clinically for various tissue repair applications [10]. SIS serves as a suitable provisional matrix for cell delivery and tissue regeneration because of its good biocompatibility and porous structure [11,12]. SIS scaffolds can also be functionalized in many ways and surface modification has been shown to enormously improve its application in tissue engineering [13]. DS-SILY, a glycan-based therapy designed to mimic decorin, is composed of collagen-binding peptides (SILY) conjugated to a dermatan sulfate (DS) backbone [14]. Decorin is a small leucine-rich proteoglycan found abundantly in skin, and is involved in maintaining regularity in collagen fibrillogenesis and preventing hypertrophic scars [15–17]. Similar to the functions of native decorin, a key feature of the DS-SILY molecule is that it binds to collagen matrices, thereby protecting the matrix from extensive and rapid proteolytic breakdown [14]. A further drawback of collagen-rich scaffolds is that they lack sufficient innate biological signals to recruit sufficient EPCs and form revascularization of ischemic wounds *in vivo*. Using One-Bead One-Compound (OBOC) combinatorial technology, an ultra-high throughput chemical library synthesis and screening method, we previously identified LXW7, a cyclic peptide ligand for the αvβ3 integrin receptor on ECs and EPCs possesses strong, stable and specific EC/EPC capturing function. and stimulates EC proliferation and phosphorylation of mitogen-activated protein kinase ERK1/2 and VEGF2 receptor (VEGFR2) [18]. Webber et al. [19] reported that grafting peptides which activate the VEGF receptor to a scaffold results in increased microcirculation and decreased hind-limb ischemia in a mouse model, highlighting the importance of VEGF receptor activation. Hence, the LXW7 peptide ligand could potentially serve to support the binding of exogenous EPCs and recruit and retain endogenous EPCs by supporting the binding of EPCs and activating the VEGFR2 receptor through engaging integrin αvβ3.

In order to assemble a functionalized skin tissue engineering scaffold that can provide a temporary residence for maintaining the angiogenic function of EPCs and support cell survival under ischemic condition, we designed a novel molecule, LXW7-DS-SILY, which is composed of both SILY and LXW7 peptides conjugated to dermatan sulfate. In a preliminary study, we first synthesized and optimized LXW7-DS-SILY variants and evaluated their proangiogenesis potential in a chick chorioallantoic membrane (CAM) model. We confirmed that LXW7-DS-SILY laden collagen hydrogels increased blood vessel formation by 43% in comparison to blank collagen hydrogels control [20]. To further explore LXW7-DS-SILY's translational potential and mechanisms of action on wound healing, we used LXW7-DS-SILY to functionalize FDA-approved, clinical-grade SIS ECM scaffolds and evaluate the therapeutic effects in a disease relevant, Zucker Diabetic Fatty (ZDF) rat ischemic skin flap model. We demonstrated that LXW7-DS-SILY functionalized ECM scaffolds increased EPC retention at the ischemic site, enhanced angiogenic function, and ultimately led to improved wound healing. A schematic diagram of the scaffold composition as well as the overall study design is illustrated in Fig. 1.

2. Materials and methods

2.1. Cell characterization and expansion

Bone marrow-derived endothelial progenitor cells (EPCs) from Zucker Diabetic Fatty (ZDF) rats were purchased from Cell Biologics, Inc. (RD-6031). EPCs were characterized by DiI-Ac-LDL staining, immunostaining of CD31 and VE-Cadherin, and tube formation assay. EPCs were cultured in complete rat endothelial cell medium (M1266, Cell Biologics). EPCs were used between passages 5 and 8 for all the experiments described in this study.

2.1.1. Lentiviral vector transduction

The lentiviral construct was generated at the University of California Davis Institute for Regenerative Cures (IRC) Vector Core. EPCs were transduced with pCCLc-MNDU3-LUC-PGK-Tomato-WPRE lentiviral vector in transduction media consisting of rat basal endothelial cell medium, 5% FBS, and 8 μg/ml protamine sulfate (MP Biomedicals) at a multiplicity of infection (MOI) of 10 for 6 h. The transduction medium was then replaced with complete rat endothelial cell medium and the cells were cultured for additional 72 h.

2.1.2. Acetylated low-density lipoprotein uptake assay

EPCs were cultured in serum-free medium for 12 h and then incubated with 10 μg/ml Dil-Ac-LDL (Alfa Aesar) for 5 h at 37 °C, 5% CO_2. Cells were then washed three times with Dulbecco's Phosphate buffered saline (DPBS, HyClone) and fixed with 10% formalin (ThermoFisher Scientific) for 15 min. The nuclei were stained with DAPI (ThermoFisher Scientific) for 5 min. Cells were washed 3 times and imaged with a Zeiss Observer Z1 microscope.

2.1.3. Tube formation assay

A 96-well plate was coated with 50 μl Matrigel (354,234, Corning) per well and incubated at 37 °C, 5% CO_2 to gel for 60 min. 1×10^4 EPCs were seeded onto the Matrigel-coated wells and incubated at 37 °C for 16 h. Phase contrast images were taken using Zeiss Observer Z1 microscope.

2.1.4. Immunofluorescent staining of rat EPCs

Cells were fixed in 10% formalin for 10 min and non-specific binding sites were blocked with 1% bovine serum albumin (BSA, bioWORLD) in 1X DPBS for 1 h at room temperature (RT). The cells were then stained with either CD31 (Abcam, ab119339, 1:200) or VE-Cadherin (ThermoFisher Scientific, 36–1900, 1:200) antibodies in 1% BSA in DPBS and incubated overnight at 4 °C. Subsequently the cells were then incubated with Alexa488 or Alexa647 conjugated secondary antibodies (ThermoFisher Scientific, 1:500) for 1 h at RT. The cell nuclei were stained with DAPI for 5 min and imaged using Zeiss Observer Z1 microscope.

2.2. EPC binding assay on LXW7-beads

For the on-bead cell binding assay, 1×10^5 EPCs were added to an ultralow attachment 24-well plate followed by addition of LXW7 resin beads. The plate was placed on shaker set at 40 rpm and incubated for 15 min at 37 °C, 5% CO_2. Phase contrast images were taken using Zeiss Observer Z1 microscope.
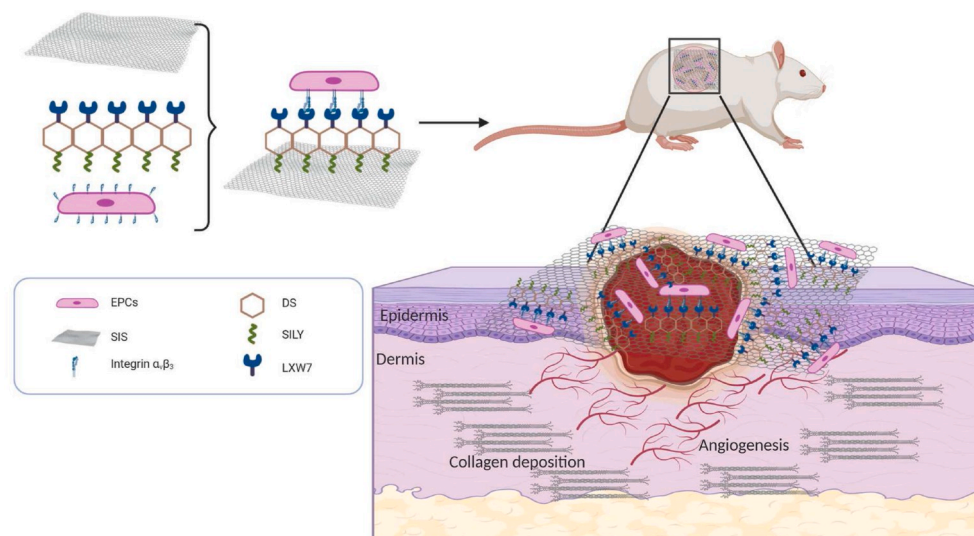
Fig. 1. Schematics for the fabrication of ligand modified scaffolds.
Multiple functional components were combined to generate a functionalized scaffold and its topical application to the site of the diabetic ischemic wound of the rat leading to improved vascularization and hastening of the healing of the damaged tissue.

2.3. Flow cytometry analysis of ligand−cell binding affinity

To quantitatively determinate ligand-cell binding affinity, flow cytometry analysis of LXW7-biotin (ligand) or D-biotin (negative control) bound to EPCs was performed, as described in our previous study [18]. Briefly, 3×10^5 EPCs were incubated with 1 μM LXW7-biotin in a binding buffer (1X HEPES (Gibco) containing 10% FBS (HyClone) and 1 mM Mn^{2+}) on ice for 30 min. The samples were washed three times with wash buffer (DPBS containing 1% FBS) and incubated with 2 μg/ml of streptavidin-PE-Cy7 conjugate (Life Technologies) on ice for 30 min and then washed with wash buffer. To test the expression of the αvβ3 integrin on EPCs, samples were stained with 20 μg/ml mouse anti-rat αvβ3 integrin antibody (Millipore Sigma) on ice for 30 min, washed three times with wash buffer, and incubated with donkey anti-mouse Alexa 647 conjugate (1:500, ThermoFisher Scientific) in DPBS on ice for 30 min and then washed with DPBS. To confirm that LXW7 binds to EPCs mainly via αvβ3 integrin, we performed a binding/blocking experiment using a monoclonal anti-αvβ3 integrin antibody. To block αvβ3 integrin, cells were first incubated with 20 μg/ml mouse anti-rat αvβ3 integrin antibody on ice for 30 min, washed three times with wash buffer, and then incubated with LXW7-biotin (1 μM) for another 30 min. The samples were washed three times with wash buffer and incubated with 2 μg/ml Streptavidin-PE-Cy7 conjugate (Life Technologies) in DPBS on ice for 30 min and then washed with DPBS. Streptavidin-PE-Cy7 only was used as the negative control. Attune NxT Flow Cytometer (ThermoFisher Scientific) was used to perform flow cytometry, and data was analyzed using FlowJo software (FlowJo LLC). The blocking efficiency of LXW7 to ZDF-EPCs was calculated according to the following formula: blocking efficiency of LXW7 to ZDF-EPCs = (B0–Bb)/B0*100, where B0 is designated as the initial ZDF-EPC-LXW7 binding percentage and Bb is designated as the ZDF-EPC-LXW7 binding percentage after ZDF-EPCs were blocked with anti-αvβ3 integrin antibody.

2.4. Synthesis and characterization of peptide-hydrazides

Hydrazide-modified peptides RRANAALKAGELYKSILYGSG-hydrazide (SILY-hydrazide) and cGRGDdvc (AEEA)$_2$WG-hydrazide (LXW7-hydrazide, wherein AEEA is short PEG linker) were synthesized using standard Fmoc solid-phase peptide synthesis according to a previously published protocol [21,22]. Briefly, Cl-TCP(Cl) ProTide Resin (loading 0.4–0.6 mmol/g, CEM Corporation) was rinsed 3 times with dichloromethane (DCM, Fisher Scientific) and N, N-Dimethylformamide

(DMF, Fisher Scientific) and swollen in 50% DCM/DMF for 1 h. Swollen resin was then reacted twice with 10% hydrazine hydrate (Sigma) in DMF and 0.057 M N, N-Diisopropylethylamine (DIPEA, Fisher Scientific) for 2 h at RT each. 10% methanol (Fisher Scientific) in DMF was used to cap any unreacted chloride groups, and the resin was washed 3 times with DMF and 3 times with DCM. The resin was then reacted with 4 equivalents of the first Fmoc-amino acid with 4 equivalents of OxymaPure, N,N-Diisopropylcarbodiimide (DIC, Fisher Scientific) and 10 equivalents of DIPEA in DMF for 4 h, followed by washing three times with DMF and three times with DCM. Subsequent amino acids were coupled for 10 min each at 50 °C on a Liberty Blue microwave peptide synthesizer (CEM Corporation) using 5 equivalents of Fmoc-amino acids, DIC, and OxymaPure with 0.1 M DIPEA. 20% piperidine in DMF was used for deprotection. Peptides were cleaved off beads using 88% trifluoroacetic acid (TFA, Fisher Scientific), 5% phenol (Sigma), 5% H2O, and 2% Triisopropylsilane (TIPS, Sigma) for 3 h. Crude peptides were precipitated in cold diethylether (Acro organics) and allowed to dry before dissolving in 5% acetonitrile/H$_2$O for purification. Before purifying, LXW7 was cyclized by oxidizing cysteine residues using ClearOx resin (Peptides International) according to manufacturer's protocol. Peptides were purified through a C18 prep column against an acetonitrile gradient on an AKTApure 25 FPLC (GE Healthcare) and confirmed by MALDI-TOF-MS (Bruker). For some experiments, peptides were purchased from InnoPep Inc.

2.5. Synthesis and characterization of molecule variants

DS-SILY or LXW7-DS-SILY were prepared by conjugating SILY-hydrazide and LXW7-hydrazide to a dermatan sulfate (DS) backbone using carbodiimide chemistry. DS (average molecular weight 41,816 Da, Celsus Laboratories) was reacted with peptide-hydrazides using 1-ethyl-3-[3-dimethylaminopropyl] carbodiimide hydrochloride (EDC, ThermoFisher Scientific) in 0.1 M MES [2- (N-morpholino) ethanesulfonic acid] buffer with 8 M urea (Sigma) and 0.6% NaCl (Sigma) titrated to pH 4.5. First, SILY-hydrazide was conjugated to the DS for 4 h using 0.01 mM EDC. The reaction was stopped by titrating the pH to 8. The product was purified using tangential flow filtration (Spectrum labs) with a 10 kDa column and then lyophilized. LXW7-hydrazide was then sequentially conjugated to the DS-SILY construct in a similar manner using 0.1 mM EDC for 24 h before purification. Peptide conjugation was verified by creating standard curves for SILY and LXW7 using concentration dependent 280 nm absorbance of aromatic amino acids and

extrapolating absorbances of synthesized molecules using readings taken on a NanoDrop UV–Vis spectrophotometer (Thermo Fisher). The structures of LXW7-DS-SILY and the reaction scheme of making LXW7-DS-SILY were described in a previous study [20].

2.6. Preparation of ligand-modified SIS scaffolds with or without EPCs

8-mm diameter punch-outs of SIS-ECM (Cook Biotech) were cut using a sterile biopsy punch and placed into wells of a 48-well plate with the rough side facing up and incubated with 0.2 ml of 10 μM LXW7-DS-SILY, DS-SILY or DPBS for 1 h at 37 °C. Scaffolds were subsequently rinsed with DPBS for three times and then soaked overnight in complete culture media at 37 °C, 5% CO_2. 5×10^5 Td-Tomato/luciferin-labeled EPCs were resuspended in 15 μl of complete media per ECM and carefully added onto the surface of LXW7-DS-SILY, DS-SILY ligand modified or unmodified SIS. The plate was placed in a 37 °C, 5% CO_2 incubator and incubated for 1 h to allow for cell adherence before addition of 0.3 ml of complete media per well.

2.7. Attachment assay and CCK-8 assay

To modify the culture surface with ligands, plates were coated with 200 μl of 20 μg/ml Avidin (Thermo Fisher) and incubated for 1 h at 37 °C. Avidin coated wells were rinsed three times with DPBS and were treated with 200 μl M equivalents (2 μM) of LXW7-biotin or D-biotin (negative control). The wells were washed three times with DPBS in 1h and blocked with 1% BSA for 1 h. After the wells were rinsed three times with DPBS, 2×10^4 EPCs were added to the wells and incubated for 20 min at 37 °C and 5% CO2. To further explore the effect of LXW7 to the binding of EPCs on an ECM scaffold surface, LXW7-DS-SILY modified SIS and untreated control SIS were placed in an ultralow attachment 48-well plate. The scaffolds were rinsed with DPBS and seeded with EPCs at a density of 1.5×10^5 cells/cm^2. After 20 min of incubation, unattached cells were washed off with DPBS three times. Images were taken using Zeiss Observer Z1 microscope. Three independent experiments were performed. Cell counter ImageJ plugin was used to determine the cell numbers in three randomly selected fields from each independent experiment.

The effect of LXW7 on the EPC growth was determined by a Cell Counting Kit-8 assay (CCK-8, Dojindo). This assay was used to detect cell viability. The 96-well plates were treated with 1 μM Avidin solution for 1 h at RT then rinsed three times with DPBS. Wells were treated with 1 μM LXW7-biotin (ligand) or 1 μM D-biotin (negative control) for 1 h, washed three times with DPBS and blocked with 1% BSA for 1 h. A total of 1.5×10^3 viable EPCs were seeded per well of the 96-well plate and cultured for 5 days. To test the growth of EPCs on LXW7-DS-SILY modified SIS scaffolds, we prepared the ligand modified scaffolds, as described above in section 2.6. A total of 5×10^4 viable EPCs were seeded per scaffold and cultured for 5 days. The CCK-8 assay was performed according to the manufacturer's instructions. Absorbance was measured at 450 nm using a SpectraMax i3 plate reader instrument (Molecular Devices LLC).

2.8. Cell loading density

The optimal loading density of EPCs on SIS-ECM was determined by the CCK-8 assay. EPCs were seeded on 8-mm SIS-ECM discs at the following densities: 0, 4.2×10^4, 1×10^5, 3×10^5, 5×10^5, and 1×10^6 cells/cm^2. At 24 h after seeding, absorbance was measured at 450 nm.

2.9. Zucker Diabetic Fatty rat ischemic skin wound model

All animal procedures were approved by the University of California, Davis (UCD) Institutional Animal Care and Use Committee (IACUC). The ligand-modified SIS scaffolds loaded with or without EPCs were prepared as described above in methods section 2.6. Male Zucker Diabetic Fatty rats (ZDF fa/fa, Charles River, 12–16 weeks old) were used and placed on a special diet to induce Type II diabetes (Purina #5008 from Lab Diet, Inc.). The blood glucose levels of ZDF rats in each group were measured using a digital glucose meter and test strips (Accu-Chek® Sensor, Roche Inc., Mannheim, Germany) 2 or 3 days prior to surgery and at the study endpoint. The rat ischemic skin wound model was carried out as previously described with some modifications [23]. The wounds created were then covered with the following SIS-scaffold treatment groups: SIS only, SIS/DS-SILY, SIS/LXW7-DS-SILY, SIS/EPCs, SIS/DS-SILY/EPCs, or SIS/LXW7-DS-SILY/EPCs (prepared as described in section 2.6). Figure S1A demonstrates the process of making Zucker Diabetic fatty rat ischemic skin wound model. The EPCs-loaded SIS scaffolds were placed with cells in direct contact with the site of the wound. Scaffolds were immobilized with 4 stitches using 5-0 silk sutures (VP710X, eSutures, Figure S1A panel g–h). To protect the wound, a Tegaderm transparent dressing (3 M Health Care, Germany) was then applied to all wounds. At days 0, 3, 7, 11, and 14 post-treatment, pictures were taken of all wounds, blinded for treatment type. The wound area was calculated by tracing the wound margins from rats and was evaluated as a percent area of the original wound using Image-Pro Plus 6.0 software. The percentage of wound reduction was calculated according to the following formula. Rate of wound closure = (A0-At)/A0*100, where A0 and At are designated as the initial wound area and wound area at the designated time, respectively.

2.10. Bioluminescence imaging

Scaffolds seeded with EPCs in the ZDF rats were monitored via In Vivo Imaging Spectrum (IVIS) system (PerkinElmer) at designated time points (1, 3, 7, and 11 days post-treatment). Prior to imaging, the rats were weighed, and luciferase substrate D-luciferin (Gold Biotechnology) was injected subcutaneously into the animals at 150 mg/kg body weight. Five min post-injection, the rats were anesthetized using 2% isoflurane for 5 min and imaged under anesthesia. Images were analyzed using Living Image®2.50 (PerkinElmer). The bioluminescence signal intensity was represented as total photons of the region of interest (ROI) subtracted by the region of no positive signal in the same animal.

2.11. Histological analysis

Animals were euthanized on day 14 and their full-thickness wound skin tissues were carefully biopsied with a 10 mm punch. The round wound tissues were cut in half vertically from the wound center then fixed with 4% paraformaldehyde for 24 h, protected by 30% sucrose dehydration for 48 h, and embedded in O·C.T compound (Sakura Finetek USA). Subsequently, sections (10 μm thick) were cut from the central wound using a Cryostat (Leica CM3050S) and stained with Hematoxylin and Eosin (H&E) to visualize tissue formation or Masson trichrome staining to observe collagen deposition during the healing period. A total of 24 single images were captured at 10X magnification, merged and analyzed using a Keyence BZ9000 microscope and the BZ II Analyzer software. A total of 5 sections from 5 rats of each group were analyzed.

For immunofluorescence staining, tissue sections were washed with DPBS, blocked with 5% BSA for 1 h in DPBS, and stained with the following primary antibodies by incubating at 4 °C overnight: RECA-1 (1:50, ab9774, mouse, Abcam), α-SMA (1:200, ab5694, rabbit, Abcam), Collagen I (1:200, ab21286, rabbit, Abcam), Collagen III (1:200, ab7778, rabbit, Abcam). Sections were then incubated with their respective secondary antibodies diluted at 1:500 for 1 h. The slides were counterstained with DAPI (1:5000) for 5 min and mounted with Prolong Diamond Antifade Mountant (Invitrogen). A Nikon A1 laser-scanning confocal microscope was used to acquire confocal images. The number of blood vessels (RECA positive) per field was counted and mean fluorescence intensity was measured by Image J. A total of 6 sections from 3 rats of each group were analyzed.

2.12. Statistics

Data are reported as mean ± standard deviation (SD) for bead-binding, block efficiency, cell attachment, CCK-8 assay and cell loading density assay and as mean ± standard error of mean (SEM) for healing rate, bioluminescence images and histological analysis. Statistical analysis of beads binding assay and cell attachment assay was performed using unpaired two-tailed distribution, equal variance student's *t*-test. Analyses of bioluminescence images, histological analysis were performed using one-way ANOVA. Healing rate analysis, CCK-8 assay was performed by two-way ANOVA. All statistical analyses were performed using PRISM 7 (GraphPad Software Inc.), and differences were considered significant when p < 0.05.

3. Results

3.1. Characterization and transduction of ZDF rat bone marrow EPCs

ZDF rat bone marrow EPCs (ZDF-EPCs) displayed the typical morphology of EPC colonies (Figure S2A) and were efficiently transduced with lentiviral vector expressing a fluorescent marker Td-tomato for tracking analysis (Figure S2B). Strong expression of EPC markers (CD31 and VE-cadherin) confirmed their EC characteristics (Figure S2C-D). The tube formation assay results revealed their ability to assemble into tubules in the presence of a basement membrane *in vitro* (Figure S2E). After co-culturing with DiI-Ac-LDL, positive staining for DiI-Ac-LDL was observed in ZDF-EPCs (Figure S2F). These results indicated that ZDF-EPCs have similar phenotype and function as human EPCs.

3.2. LXW7 ligand showed excellent binding affinity to ZDF-EPCs via the αvβ3 integrin

In our previous studies, we identified LXW7 as a potent ligand that specifically targets EPCs and ECs normally present in circulation via binding to αvβ3 integrin on cell surfaces [18,24]. To confirm the binding of LXW7 to the ZDF-EPCs, resin beads displaying LXW7 were incubated with ZDF-EPCs. Monocyte cell line THP-1 served as a negative control.

After 30 min of incubation, the LXW7 beads showed strong binding to ZDF-EPCs but not to THP-1 monocytes (Fig. 2A). Quantification of the number of cells bound on each bead showed that there was a significant increase in the binding of ZDF-EPCs to LXW7 resin beads compared to THP-1 monocytes (Fig. 2B). To further confirm that LXW7 binds to ZDF-EPCs mainly via αvβ3 integrin, we performed flow cytometry analysis to detect the expression of αvβ3 integrin and performed a binding/blocking experiment using a monoclonal anti-αvβ3 integrin antibody. The results showed αvβ3 integrin was expressed on the majority of ZDF-EPCs [(75.33 ± 4.25% of overall populations) Fig. 2C]. From the binding/blocking experiment, as shown in Fig. 2D, we confirmed that LXW7 had high binding efficiency to ZDF-EPCs, and LXW7 binding to ZDF-EPCs was blocked by the anti-αvβ3 integrin antibody (Fig. 2D). The average blocking efficiency was 60.8 ± 22.1% (Fig. 2D). These data confirmed that the binding of LXW7 to ZDF-EPCs was primarily mediated via αvβ3 integrin.

3.3. LXW7 modified surfaces increased ZDF-EPC attachment and growth

To determine if the LXW7 ligand can support effective ZDF-EPC attachment and growth, we employed both 2D tissue culture surfaces and 3D ECM-based scaffolds to determine cell-ligand binding ability in different situations. We treated tissue culture polystyrene with LXW7-biotin (ligand) or D-biotin (negative control) and investigated selective attachment of ZDF-EPCs. To further explore the binding ability of LXW7 to ZDF-EPCs on ECM-based scaffolds, we incubated LXW7-DS-SILY with SIS to allow binding of the biofunctional ligand to the SIS. Seeding ZDF-EPCs on both the 2D and 3D surfaces showed that LXW7 and LXW7-DS-SILY can support attachment of ZDF-EPCs both to plate and SIS surfaces (Fig. 3A, 3B, 3D, 3E). The number of cells attached was quantified and the results demonstrated that the LXW7-treated surfaces attracted more ZDF-EPCs than the unmodified surfaces (Fig. 3C and F respectively).

The effect of LXW7 on the growth of ZDF-EPCs was tested by CCK-8 assay at different time points in a course of 5 days. Results showed that the LXW7-biotin treated surface significantly promoted the growth of
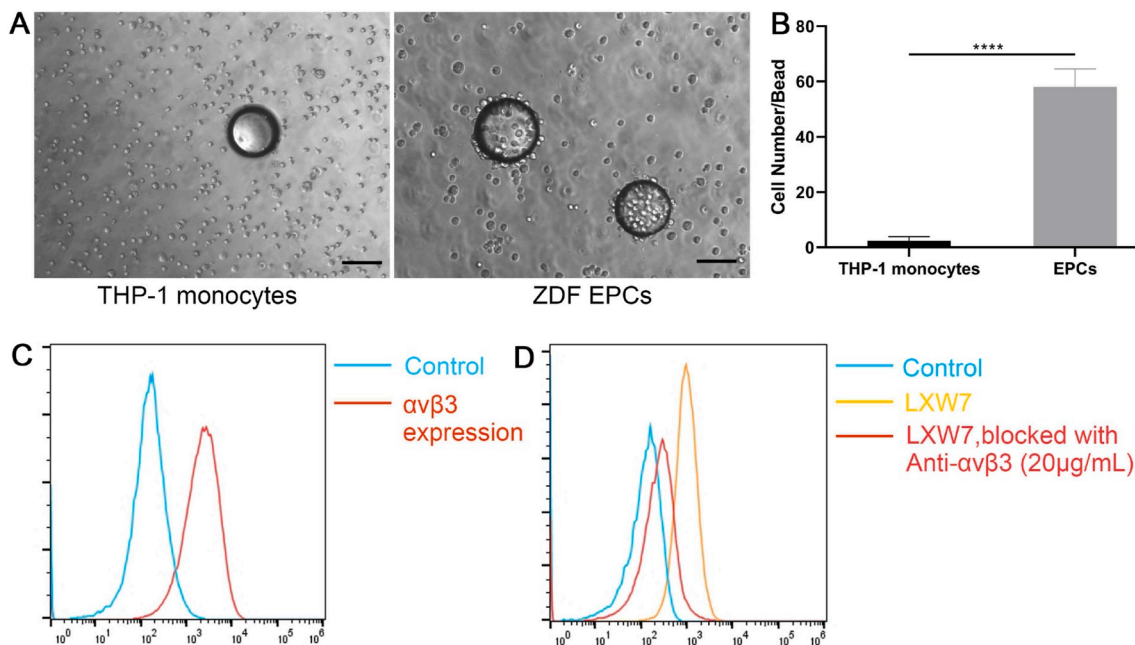

Fig. 2. Specificity and binding affinity of LXW7 ligand to ZDF-EPCs and expression of αvβ3 integrin on ZDF-EPCs
A. On-bead cell binding assay for testing the binding affinity and specificity of ligands to ZDF-EPCs showing high binding of ZDF-EPCs to LXW7 coated beads (right panel) compared to THP-1 monocytes (left panel). **B.** Quantification of the number of THP-1 monocytes and ZDF-EPCs bound to the LXW7 coated beads. **C.** Expression of αvβ3 integrin on ZDF-EPCs. **D.** Flow cytometry analysis of the binding affinity of LXW7 showing the blocking of its binding by anti-αvβ3 antibody. Scale bar = 100 μm. Data are expressed as mean ± SD. ****p < 0.0001, n = 3.

ZDF-EPCs after 48 h in culture compared with the D-biotin treated surface (control), and this trend was maintained for the entire period of the experiment (Fig. 3G). Similar to the trend on tissue culture plates, SIS/LXW7-DS-SILY also promoted the growth of ZDF-EPCs when compared to SIS/DS-SILY and SIS (Fig. 3H). These results demonstrate that the LXW7-modified surface and functionalized scaffold support attachment and growth of EPCs.

3.4. In vivo wound healing studies

A bipedicle cutaneous flap was created on each rat to yield 2 ischemic and 2 non-ischemic wounds per animal (Figure S1A, S1B). Both ischemic and non-ischemic wounds were implanted with ligand-modified or un-modified SIS patches seeded with or without ZDF-EPCs at a seeding density of 5×10^5 cells/cm^2. This seeding density was based on the result obtained from our CCK-8 assay where a decrease in cell viability was observed beyond a density of 5×10^5 cells/cm^2 (Figure S3). The average blood glucose level of ZDF rats in each group >250 mg/dl.

3.4.1. LXW7-DS-SILY modified SIS scaffolds accelerated diabetic non-ischemic wound healing and supported survival of ZDF-EPCs

The diabetic wound healing assay was performed to evaluate the effect of the different scaffolds on non-ischemic wound healing *in vivo*. The wound regions of the diabetic rat were treated with SIS/LXW7-DS-SILY/EPCs, SIS/DS-SILY/EPCs, SIS/EPCs, SIS/LXW7-DS-SILY, SIS/DS-SILY and SIS respectively. Digital photographs were obtained 0, 3, 7, 11, and 14 days after surgery (Fig. 4A). In the absence of exogenous ZDF-EPC seeding, the wound area in all groups decreased over time, and the average observed wound closure rate was significantly increased in the SIS/LXW7-DS-SILY group (80.7 ± 2.6%) compared to both the SIS/DS-SILY (56.9 ± 1.3%) and SIS (56.3 ± 4.7%) groups on day 14 (Fig. 4B panel a). Among all groups loaded with exogenous ZDF-EPCs, the group treated with SIS/LXW7-DS-SILY/EPCs showed a wound healing rate of

82.5 ± 1.6%, significantly higher than that of SIS/DS-SILY/EPCs (69.7 ± 2.5%) and SIS/EPCs (67.2 ± 2.8%) groups (Fig. 4B panel b). However, in the non-ischemic wounds, ZDF-EPCs did not accelerate wound closure when comparing SIS/LXW7-DS-SILY/EPCs with SIS/LXW7-DS-SILY or comparing SIS/EPCs with SIS. When compared to SIS/DS-SILY, SIS/DS-SILY/EPCs accelerated wound healing (Fig. 4B panel c–e).

To investigate cell survival of transplanted cells in ZDF rats, Td-Tomato/luciferin-labeled ZDF-EPCs were seeded on different scaffolds and monitored by IVIS. The bioluminescence signal in the SIS/LXW7-DS-SILY/EPCs group showed a significantly higher intensity when compared to SIS/DS-SILY/EPCs and SIS/EPCs groups at days 1, 3 and 7, suggesting that LXW7 improved ZDF-EPC retention in the wound bed at early time points (Fig. 4C). The intensity in all the three groups decreased to baseline by day 11 (Fig. 4D).

3.4.2. LXW7-DS-SILY modified SIS scaffolds accelerated wound healing and re-epithelialization in non-ischemic wound areas

To further compare the healing quality of wounds treated by different scaffolds, H&E staining was performed on non-ischemic wound tissue samples (Fig. 5A). As shown in Fig. 5C, the SIS/LXW7-DS-SILY/EPCs group showed the shortest residual wound length among all the groups, followed by SIS/LXW7-DS-SILY, SIS/DS-SILY/EPCs, SIS/EPCs, SIS and SIS/DS-SILY groups at day 14. SIS/LXW7-DS-SILY showed a significantly shorter wound length compared to SIS/DS-SILY and SIS groups with or without EPCs (Fig. 5C panel a–b). Also, the SIS/LXW7-DS-SILY/EPCs and SIS/DS-SILY/EPCs groups were fully covered with neoepidermis, while in the other groups, re-epithelialization was not fully completed (Fig. 5D). Overall, the SIS/LXW7-DS-SILY/EPCs group showed a higher efficacy of wound healing in comparison with other groups.

3.4.3. LXW7-DS-SILY modified SIS scaffolds promoted neovascularization and stimulated collagen deposition in non-ischemic wound areas

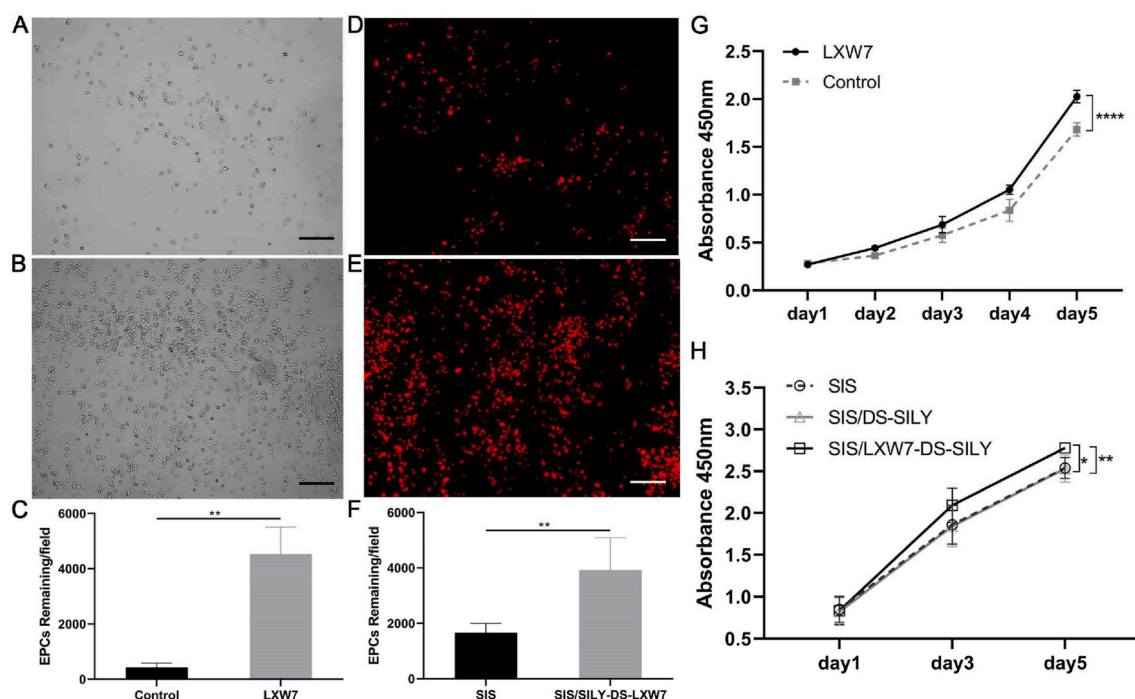To evaluate neovascularization, we morphometrically assessed blood

Fig. 3. Effect of LXW7 and LXW7-DS-SILY ligands on the attachment, growth and viability of ZDF-EPCs on ligand modified surfaces.
A-B. Representative images of attached ZDF-EPCs on surfaces treated by D-biotin (A; control), LXW7 (B) after 20 min incubation. **C.** Quantification and the correlative statistical analysis of remaining cells shown in **A-B**. **D-E.** Representative images of adhered EPCs on untreated (D; control) or LXW7-DS-SILY modified SIS surface (E) after 20 min incubation. **F.** Quantification and the correlative statistical analysis of remaining cells shown in **D-E**. **G.** Growth and viability of ZDF-EPCs on LXW7 treated tissue culture surfaces and D-biotin treated surfaces (control) was assessed by CCK-8 assay. **H.** Growth and viability of ZDF-EPCs on LXW7-DS-SILY or DS-SILY treated SIS scaffold surfaces was assessed by CCK-8 assay. Scale bar = 200 μm. Data are expressed as mean ± SD. ****p < 0.0001, **p < 0.01, *p < 0.05, n = 3.
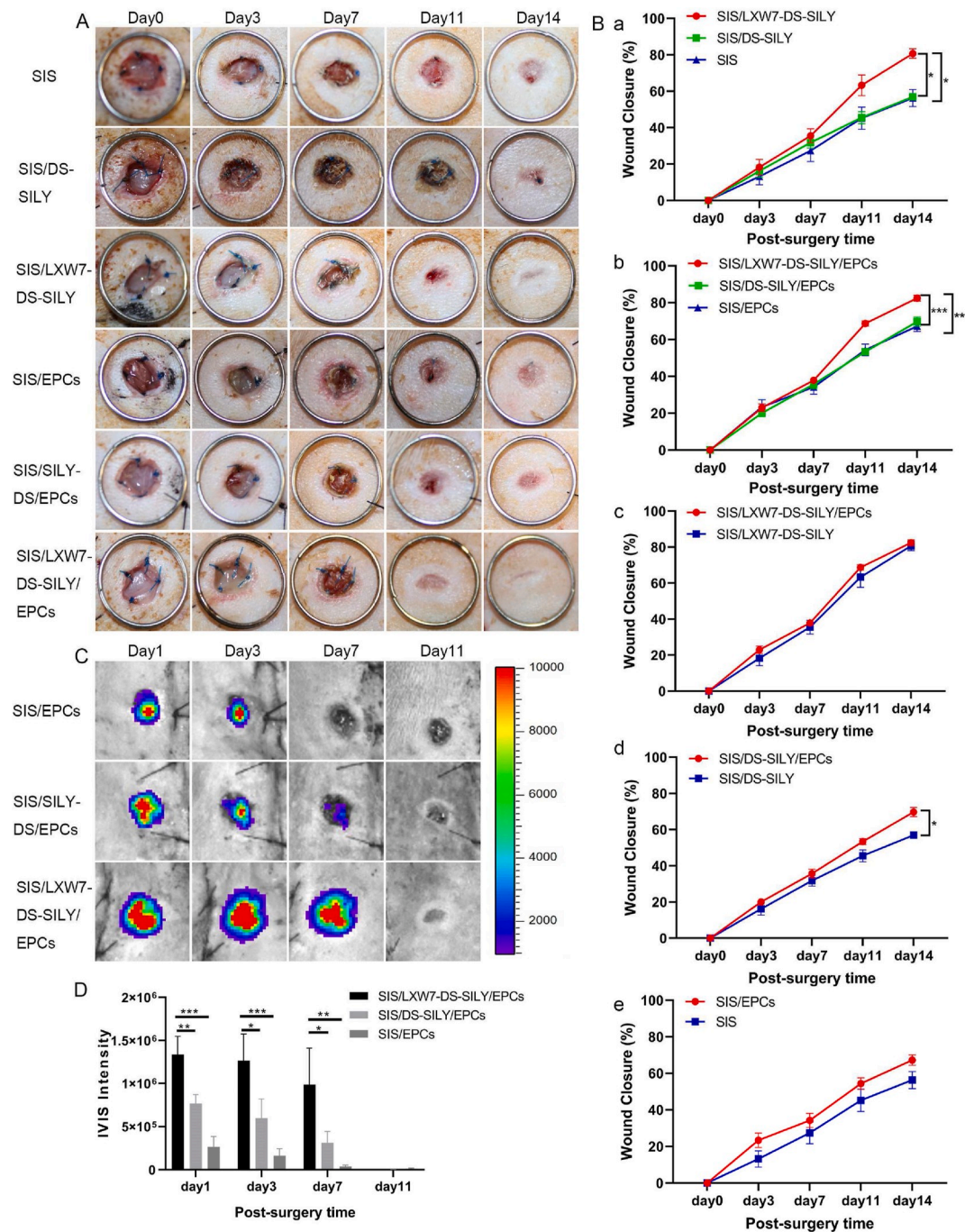
Fig. 4. SIS/LXW7-DS-SILY scaffolds accelerate wound closure and support ZDF-EPC survival under non-ischemic condition.
A. Representative images of healing in wounds treated with different groups at days 0, 3, 7, 11 and 14. **B**. Quantification of the healing rate of different groups. a) SIS/LXW7-DS-SILY group was significantly better compared to SIS/DS-SILY and SIS groups. b) SIS/LXW7-DS-SILY/EPCs group was significantly better than the SIS/DS-SILY/EPCs and SIS/EPCs groups. c) SIS/LXW7-DS-SILY/EPCs group compared to SIS/LXW7-DS-SILY group showed no significant difference. d) SIS/DS-SILY/EPCs group was significantly better compared to SIS/DS-SILY group. e) There was a trend that the SIS/EPCs group was better than the SIS group but the difference was not statistically significant. Data are expressed as mean ± SEM. SIS group, SIS/LXW7-DS-SILY group, and SIS/EPCs group: n = 8; SIS/DS-SILY group: n = 7; SIS/DS-SILY/EPCs group: n = 12; SIS/LXW7-DS-SILY/EPCs group: n = 13. **C**. Bioluminescence imaging of wounds transplanted with different modified SIS scaffolds loaded with Td-Tomato/luciferin-labeled ZDF-EPCs. **D**. Quantification of the signal intensity of bioluminescence (Most of the SIS scaffolds spontaneously fall off the wounds by day 11). Data are expressed as mean ± SEM. n = 5 per group. ***$p < 0.001$, **$p < 0.01$, *$p < 0.05$.

vessel density at wound sites using immunostaining for rat anti-endothelial cell antibody-1 (RECA-1) and alpha-smooth muscle actin (α-SMA) at day 14 (Fig. 6A). Wounds treated with SIS/LXW7-DS-SILY scaffold showed a significantly higher vessel number than SIS/DS-SILY and SIS scaffolds in the regenerated tissue (Fig. 6D panel a). When wounds were treated with different scaffolds seeded with ZDF-EPCs, SIS/LXW7-DS-SILY/EPCs promoted neovascularization compared to control scaffolds with ZDF-EPCs

(Fig. 6D panel b). In addition, blood vessels in the SIS/LXW7-DS-SILY/EPCs group displayed a mature structure with a larger lumen when compared to control groups (Fig. 6A).

To observe collagen morphology and distribution, Masson Trichrome staining was conducted. Masson staining showed arrangement of newly formed collagen in the regenerated tissue in all six groups (Fig. 5B). On day 14, densely packed and basket-weave patterns typical of collagen fibers were
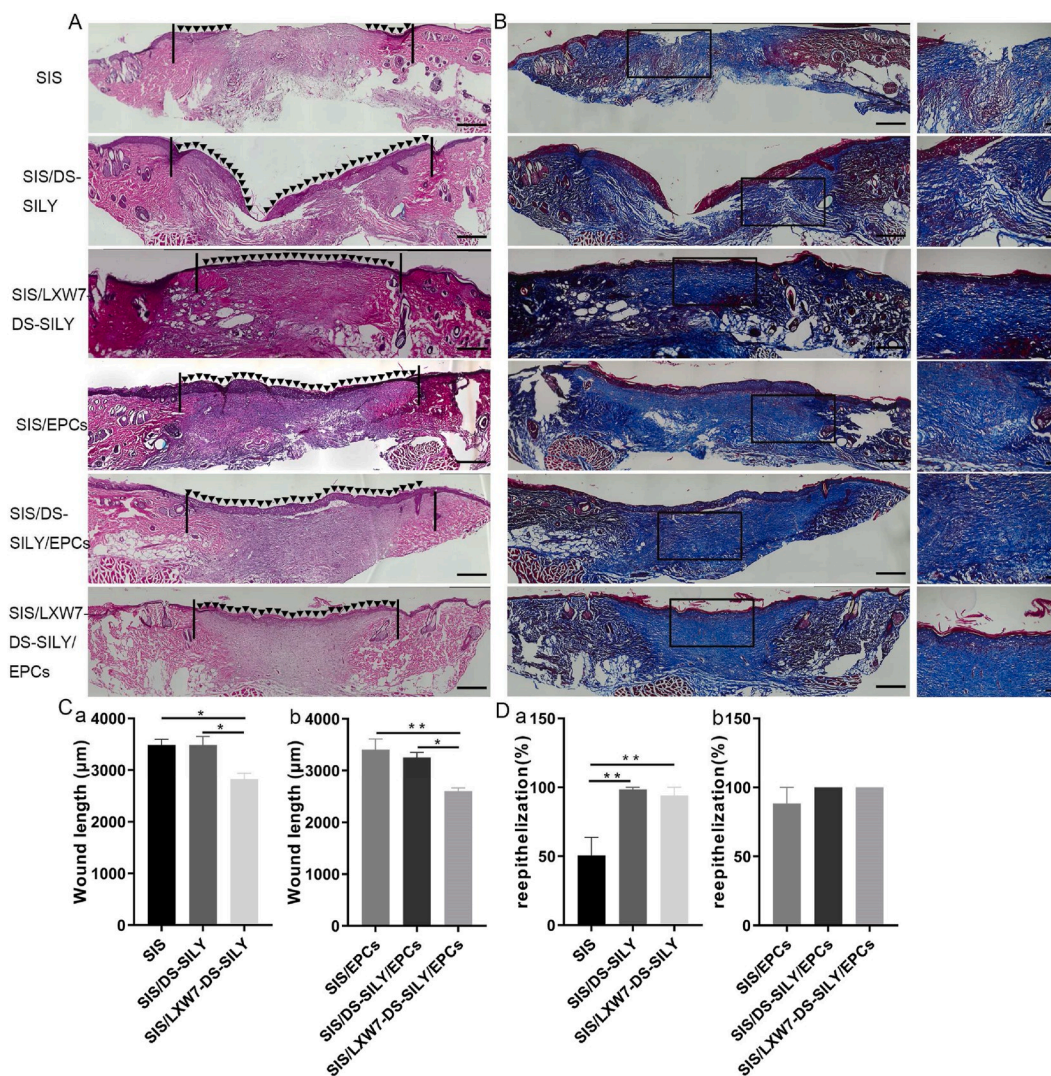
Fig. 5. Histology evaluation of wounds treated by different scaffolds under non-ischemic condition.
A. Representative images of H&E staining of wounds at day 14 under non-ischemic condition. The area indicated by the black arrows represents the newly formed epidermis of the wound area. The black lines indicate the leading wound edges. **B.** Representative images of Masson Trichrome staining of wounds at day 14. Collagen stains blue, nuclei stain dark brown, whereas muscle, cytoplasm and keratin stain red. The higher magnification image on the right shows the insert of the lower magnification image in each respective group. **C-D.** Quantification of the wound length (C) and percentage of re-epithelization (D) of different modified SIS scaffolds. Data are expressed as mean ± SEM. **$p < 0.01$, *$p < 0.05$, n = 5 per group. Original scale bar = 500 μm and close-up scale bar = 200 μm.

observed for the SIS/LXW7-DS-SILY/EPCs group while only sparse, loosely packed collagen fibers were observed in the SIS-only group (Fig. 5B).

To detect whether the collagen deposition could be stimulated by the various treatment groups, collagen immunostaining of the tissue sections was performed. Enhanced collagen I and collagen III staining intensity was observed in SIS/LXW7-DS-SILY/EPCs treated wounds on day 14, compared to the other wounds (Fig. 6B and C). SIS/LXW7-DS-SILY also showed a significantly higher collagen I and III staining intensity compared to SIS/DS-SILY and SIS groups with or without EPCs (Fig. 6E–F, panel a–b).

3.4.4. LXW7-DS-SILY modified SIS scaffolds accelerated diabetic ischemic wound healing and supported ZDF-EPC survival

To detect the effect of the different scaffolds on wound healing under ischemic conditions, we treated the ischemic wounds with SIS/LXW7-DS-SILY/EPCs, SIS/DS-SILY/EPCs, SIS/EPCs, SIS/LXW7-DS-SILY, SIS/DS-SILY or SIS. Digital photographs were obtained 0, 3, 7, 11, and 14 days after the operation (Fig. 7A). The wound area in all groups decreased over time and the average observed wound closure rate was significantly higher in the SIS/LXW7-DS-SILY group (44.1 ± 4.8%), compared with SIS group (30.0 ± 5.5%) at day 14 (Fig. 7B panel a). There was no difference between the SIS/DS-SILY (46.3 ± 7.7%) and the SIS/LXW7-DS-SILY group (44.1 ± 4.8%) or

SIS group (30.0 ± 5.5%). With respect to all groups loaded with ZDF-EPCs, the wounds treated with SIS/LXW7-DS-SILY/EPCs showed a wound closure rate of 61.6 ± 4.7%, significantly higher than that of the SIS/DS-SILY/EPCs (43.5 ± 5.2%) and SIS/EPCs (34.8 ± 5.0%) groups. There was no difference between SIS/DS-SILY/EPCs and SIS/EPCs groups (Fig. 7B panel b). Finally, the SIS/LXW7-DS-SILY/EPCs group showed a significantly higher healing rate than the SIS/LXW7-DS-SILY group highlighting the importance of the ZDF-EPCs in ischemic wound healing (Fig. 7B panel c). No significant difference was observed when comparing SIS/DS-SILY/EPCs with SIS/DS-SILY or comparing SIS/EPCs with SIS (Fig. 7B panel d–e).

To investigate cell survival of transplanted cells in ischemic wounds, Td-Tomato/luciferin-labeled ZDF-EPCs were seeded on different scaffolds and imaged by IVIS (Fig. 7C). The bioluminescence signal in SIS/LXW7-DS-SILY/EPCs group only showed a significantly higher intensity when compared to SIS/EPCs group at day 1. The intensity in all three groups decreased to baseline by day 11 (Fig. 7D).

3.4.5. LXW7-DS-SILY modified SIS scaffolds accelerated wound healing and re-epithelialization in ischemic wound areas

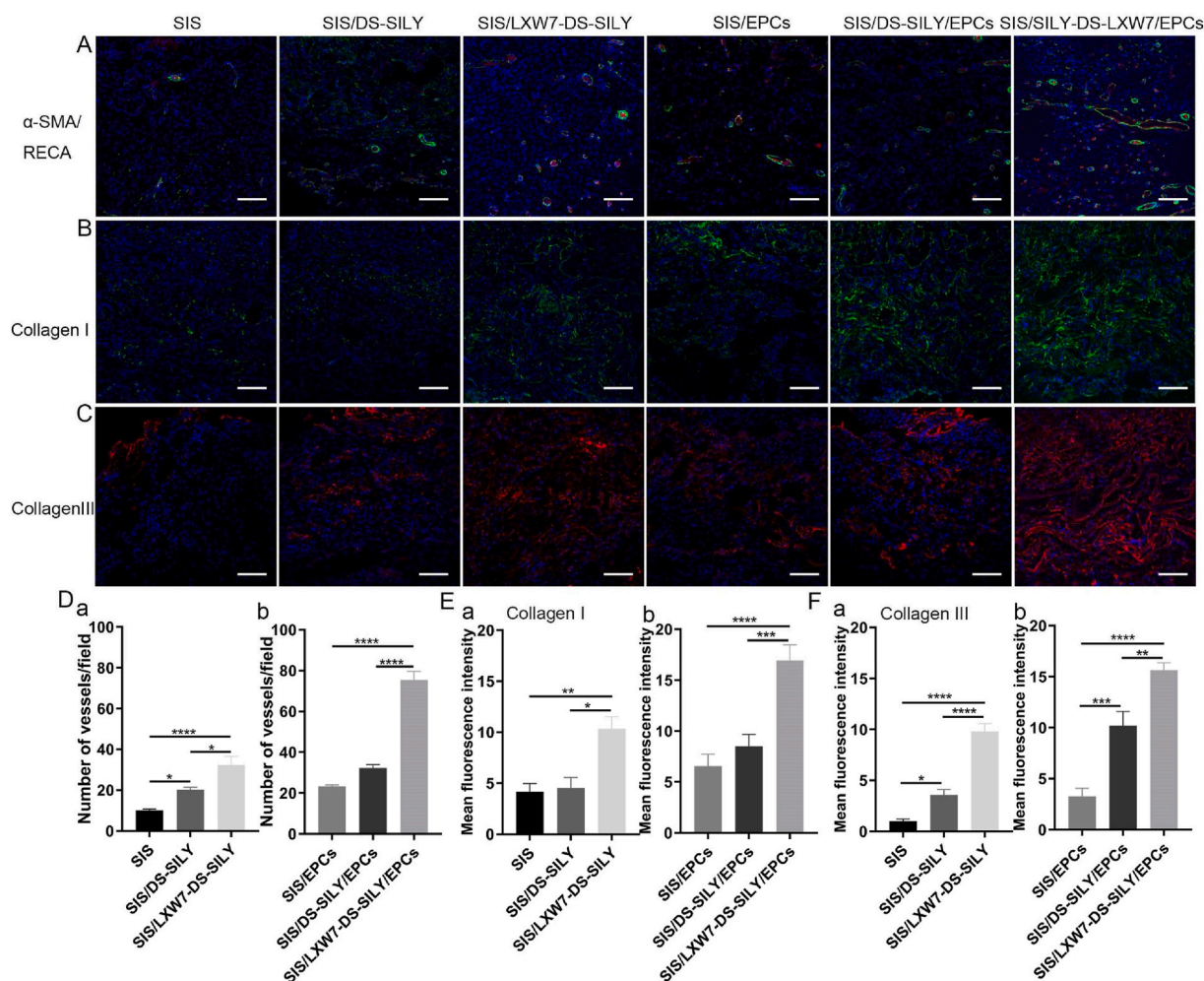Overall, the wound healing quality of ischemic wounds is much worse

Fig. 6. Neovascularization and collagen deposition evaluation of wounds treated by different scaffolds under non-ischemic condition.
A. Blood vessels stained with α-SMA (green) and RECA (red) in wound bed at day 14 post surgery. **B–C.** Immunostaining of collagen I and collagen III expression in wound bed at day 14 post surgery. **D-F.** Quantification of the number of blood vessels/field (D), immunofluorescence intensity of collagen I (E) and collagen III (F). Data are expressed as mean ± SEM. **p < 0.01, *p < 0.05, n = 3 per group. Scale bar = 100 μm.

than in non-ischemic wounds (Fig. 8A). The SIS/LXW7-DS-SILY/EPCs group showed a trend toward more rapid re-epithelialization as compared to the SIS/EPCs group, as determined by shorter residual wound length (Fig. 8C–D panel b). However, no significant differences on wound length were found between the SIS/LXW7-DS-SILY/EPCs and SIS/DS-SILY/EPCs groups (Fig. 8C panel b). Without EPCs, SIS/LXW7-DS-SILY scaffolds alone still have a positive effect on wound length and re-epithelialization when compared to the SIS group (Fig. 8C panel a, Fig. 8D panel a).

3.4.6. LXW7-DS-SILY modified SIS scaffolds promote angiogenesis and stimulate collagen deposition in ischemic wounds

To evaluate ischemic wound angiogenesis, we stained tissue sections for RECA-1 and α-SMA to assess capillary densities at day 14 (Fig. 9A). Wounds treated with SIS/LXW7-DS-SILY scaffolds showed a significantly higher vessel number than SIS/DS-SILY and SIS scaffolds in the regenerated tissue (Fig. 9D panel a). When wounds were treated with different scaffolds seeded with ZDF-EPCs, SIS/LXW7-DS-SILY/EPCs promoted angiogenesis more than the other two groups (Fig. 9D panel b).

The result showed that irregular and fewer collagen fibers were formed during this time point for the SIS group as compared to other groups (Fig. 8B). Enhanced collagen I and collagen III staining intensity was observed in SIS/LXW7-DS-SILY/EPCs treated wounds on day 14 when compared to the other wounds (Fig. 9B and C). SIS/LXW7-DS-SILY showed a significantly higher collagen III intensity than the SIS/DS-SILY and SIS groups, and a higher collagen I intensity than the SIS group (Fig. 9E–F,

panel a). When wounds were treated with different scaffolds seeded with EPCs, SIS/LXW7-DS-SILY/EPCs showed significantly higher expression of collagen I and collagen III than the other two groups (Fig. 9E–F panel b).

4. Discussion

It is well established that impaired healing of diabetic wounds is affected by several factors, such as hypoxia, dysfunction of fibroblasts and epidermal cells, impaired angiogenesis and neovascularization, and high levels of metalloproteases [25,26]. Hyperinsulinemia in diabetic patients impairs the proliferation and tube formation of EPCs [27]. Stem cells and regenerative materials exhibit potentially therapeutic effects towards wound and tissue regeneration. Different engineering strategies have been developed to improve stem cell retention and survival at the wound sites such as using the injectable nano-in-micro hydrogel system [28], biomolecules modified biosynthetic scaffolds [29], and magnetic nanoparticle-embedded hydrogel sheet [30]. Adult stem cells such as EPCs, adipose tissue derived stem cells (ADSCs) and mesenchymal stromal/stem cells (MSCs) have been widely used for wound healing applications [5,31]. There are several potential key differences between EPCs and ADSCs/MSCs for wound healing. Based on our own experiences and literature, in general, adult ADSCs/MSCs do not tend to persist following transplantation and thus unlikely contribute to tissue regeneration by integration [32–34]. It is generally accepted that the main regenerative effects of MSCs result from paracrine mechanisms mediated by secreted factors, including extracellular vesicles such as exosomes and
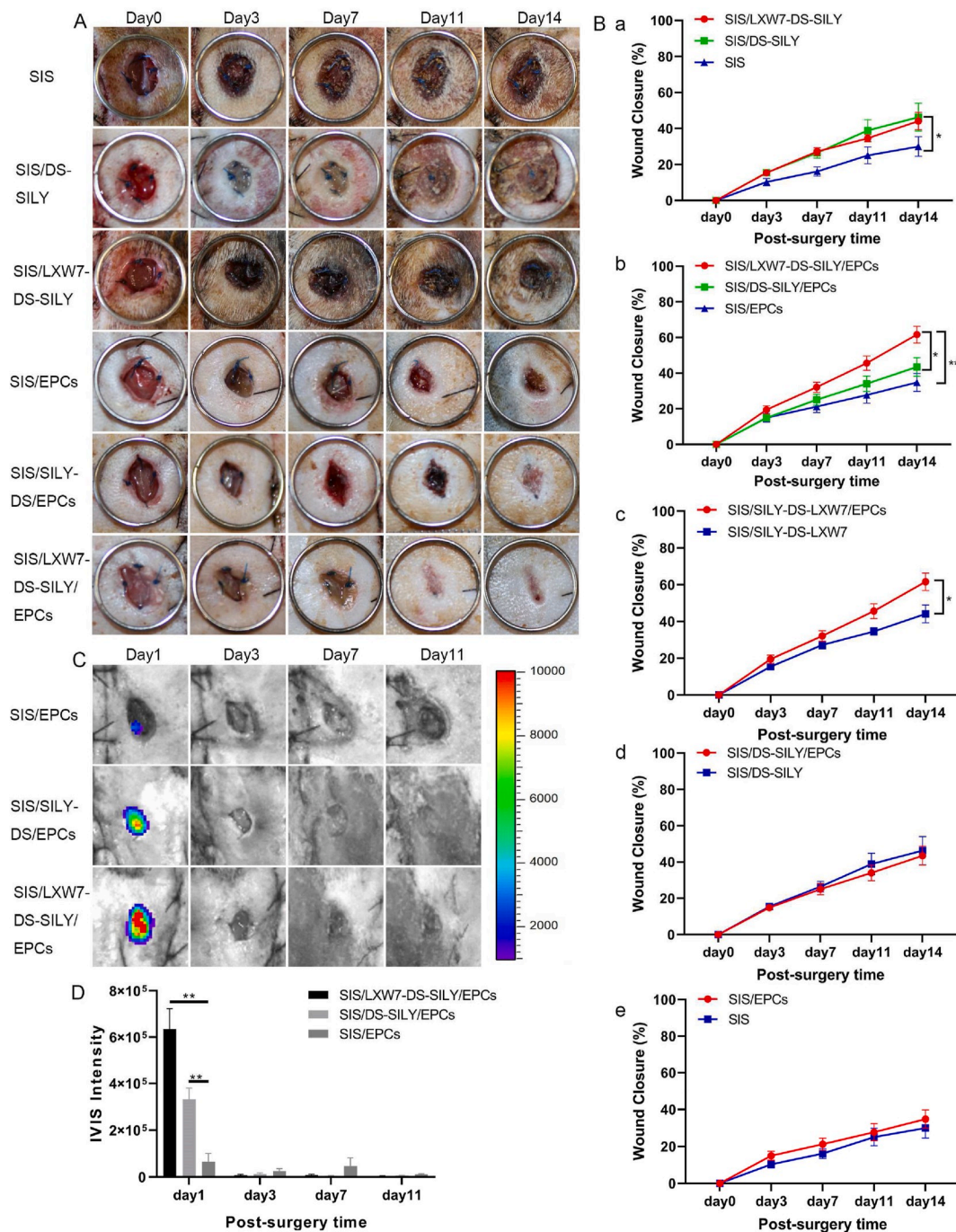
Fig. 7. SIS/LXW7-DS-SILY constructs accelerate wound closure and support survival of ZDF-EPCs under ischemic condition.
A. Representative images of healing in wounds treated with different groups at days 0, 3, 7, 11 and 14. **B.** Quantification of the wound closure rates of different groups. a) SIS/LXW7-DS-SILY group was significantly better compared to SIS group. There was a trend that the SIS/DS-SILY group was better than the SIS group but the difference was not statistically significant. b) SIS/LXW7-DS-SILY/EPCs group was significantly better than the SIS/DS-SILY/EPCs and SIS/EPCs groups. c) SIS/LXW7-DS-SILY/EPCs group was significantly better compared to SIS/LXW7-DS-SILY group. d) SIS/DS-SILY/EPCs group compared to SIS/DS-SILY group showed no significant difference. e) SIS/EPCs group compared to SIS group showed no significant difference. Data are expressed as mean ± SEM. SIS group, SIS/LXW7-DS-SILY group, and SIS/EPCs group: n = 8; SIS/DS-SILY group: n = 7; SIS/DS-SILY/EPCs group: n = 11; SIS/LXW7-DS-SILY/EPCs group: n = 12. C. Bioluminescence image of wounds transplanted with different modified scaffolds loaded with ZDF-EPCs. D. Quantification of the bioluminescence signals intensity (Most of the SIS scaffolds spontaneously fall off the wounds by day 11). Data are expressed as mean ± SEM. n = 5 per group. **p < 0.01, *p < 0.05.

microvesicles [35–37]. Additionally, MSCs have also demonstrated the ability to regulate the immune system through multiple independent pathways [38] which may facilitate wound healing. On the other hand, EPCs can engraft and become part of the neovasculature if the environment is permissive [39–41]. EPCs could also secrete angiogenic growth factors that may facilitate wound healing [42]. In the current study, the transplanted EPCs may be activated by LXW7 and the other environmental cues in the

wound sites and secrete biomolecules that support angiogenesis from the existing blood vessels. The endogenous EPCs at the wound sites will also secrete paracrine factors that will stimulate the surrounding tissues and cells and thus promote angiogenesis and improve wound healing. More detailed studies on EPC secretome and its function on wound healing are warranted.

The streptozotocin (STZ)-induced diabetic rodent model with non-ketosis hyperglycemia is the most widely used model for the
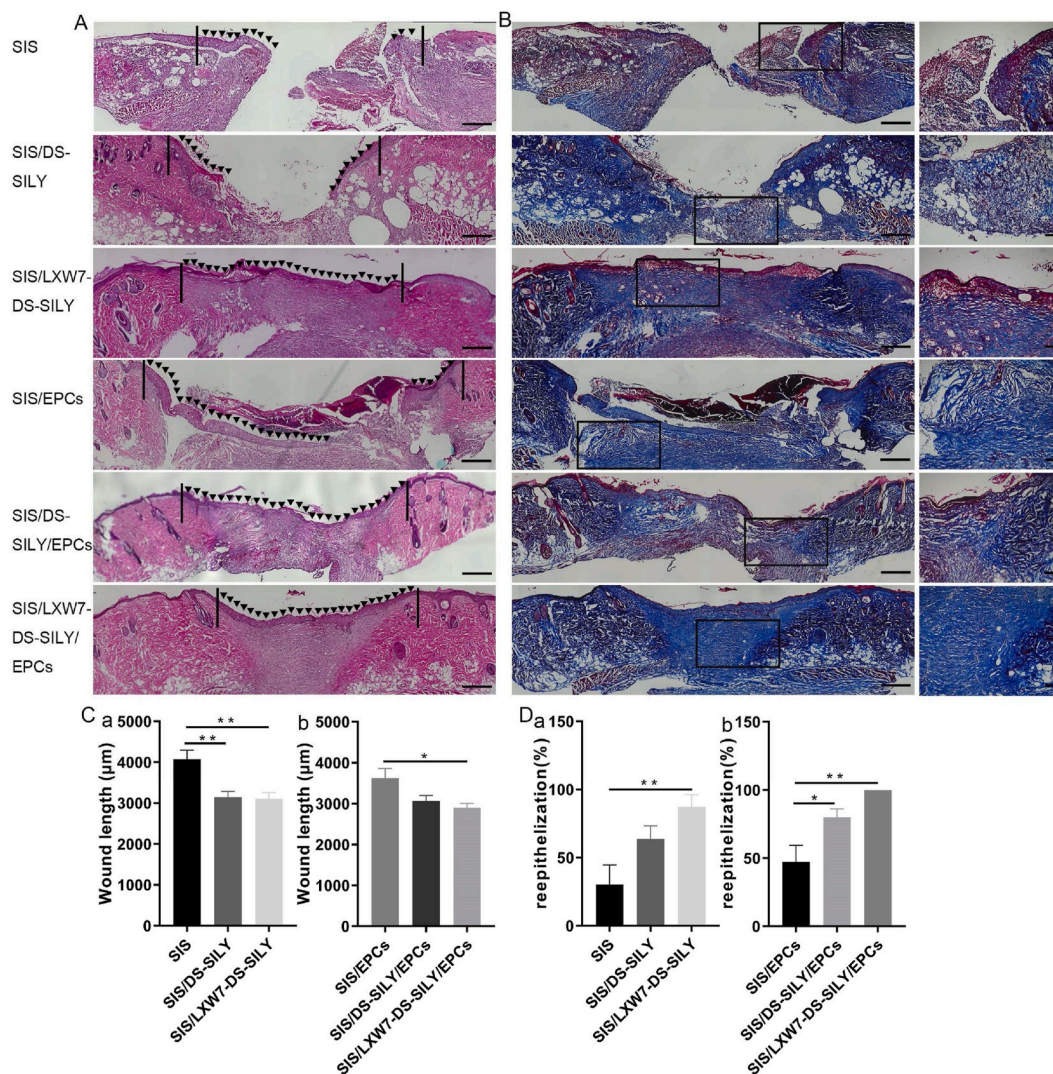
Fig. 8. Histology evaluation of wounds treated by different scaffolds under ischemic condition.
A. Representative images of H&E staining of wounds at day 14 under ischemic condition. The area indicated by the black arrows represents the newly formed epidermis of the wound area. The black lines indicate the leading wound edges. **B.** Representative images of Masson Trichrome staining of wounds at day 14. Collagen stains blue, nuclei stain dark brown, whereas muscle, cytoplasm and keratin stain red. The higher magnification image on the right shows the insert of the lower magnification image in each respective group. **C-D.** Quantification of the wound length (C) and re-epithelization rates (D) of different groups. Data are expressed as mean ± SEM. **p < 0.01, *p < 0.05, n = 5 per group. Original scale bar = 500 μm and close-up scale bar = 200 μm.

pathogenesis of type 1 diabetes research [43]. However, the STZ model induced type 1 diabetes have some limitations such as organ toxicity, low stability, and impaired weight gain in animals [44]. Since type 2 diabetes account for the majority of patients with diabetes, and given the prevalence of ischemic wounds in type 2 diabetic patients, animal models that better recapitulate the pathophysiological situations of type 2 diabetic ischemic wounds serve as a better option for evaluating the function of innovative treatments for diabetic ischemic wound healing. In this study, we designed and developed a regenerative bioscaffold (SIS/LXW7-DS-SILY) loaded with EPCs and tested the therapeutic efficacy by localized topical application of the scaffold at excisional wound sites that were created to mimic the highly ischemic condition of the clinical DFU. We chose to use the Zucker diabetic fat (ZDF) rat model to evaluate the therapeutic effects of the regenerative treatment for diabetic ischemic wounds. The ZDF rat is a well-characterized model of the metabolic syndrome and the pathophysiologic mechanism of this model is attributed to the missense mutation of leptin receptor [44,45]. ZDF rats exhibit obesity with diabetes and are characterized by hyperglycemia, insulin resistance, hyperlipidemia and impaired glucose tolerance [45], accompanied with delayed wound healing, impeded blood flow,

and diabetic nephropathy [46–48]. ZDF rats become obese at around 4 weeks of age and develop type 2 diabetes at 8–12 weeks of age [46]. Additionally, in order to mimic the highly ischemic condition of the clinical DFU in this diabetic rat model, we inserted a silicone sheet beneath the pedicle flap containing the excisional wound to ensure no reperfusion from underlying tissue [23].

The wound healing mechanisms between rodents and humans are different due to anatomical variations. In rodents, healing occurs by wound contraction because of the paniculosus carnosus layer that is situated directly below the skin. In contrast, wound healing in humans occurs via re-epithelization and granulation tissue formation [49]. However, Slavkovsky, et al. [46] showed that the contraction of diabetic wounds in ZDF rats is impaired, and wound healing predominantly occurs by re-epithelialization at the wound site. To mimic this in our study, scaffolds were immobilized to the wounds with silk threads which can reduce wound contraction or enlargement. Together, the ZDF rat model developed in this study is an effective model to study the therapeutic efficacy of functionalized scaffolds for human diabetic ischemic wound healing.

Using this model, we showed that under the non-ischemic condition, the SIS/LXW7-DS-SILY/EPCs group displayed a significantly faster rate of
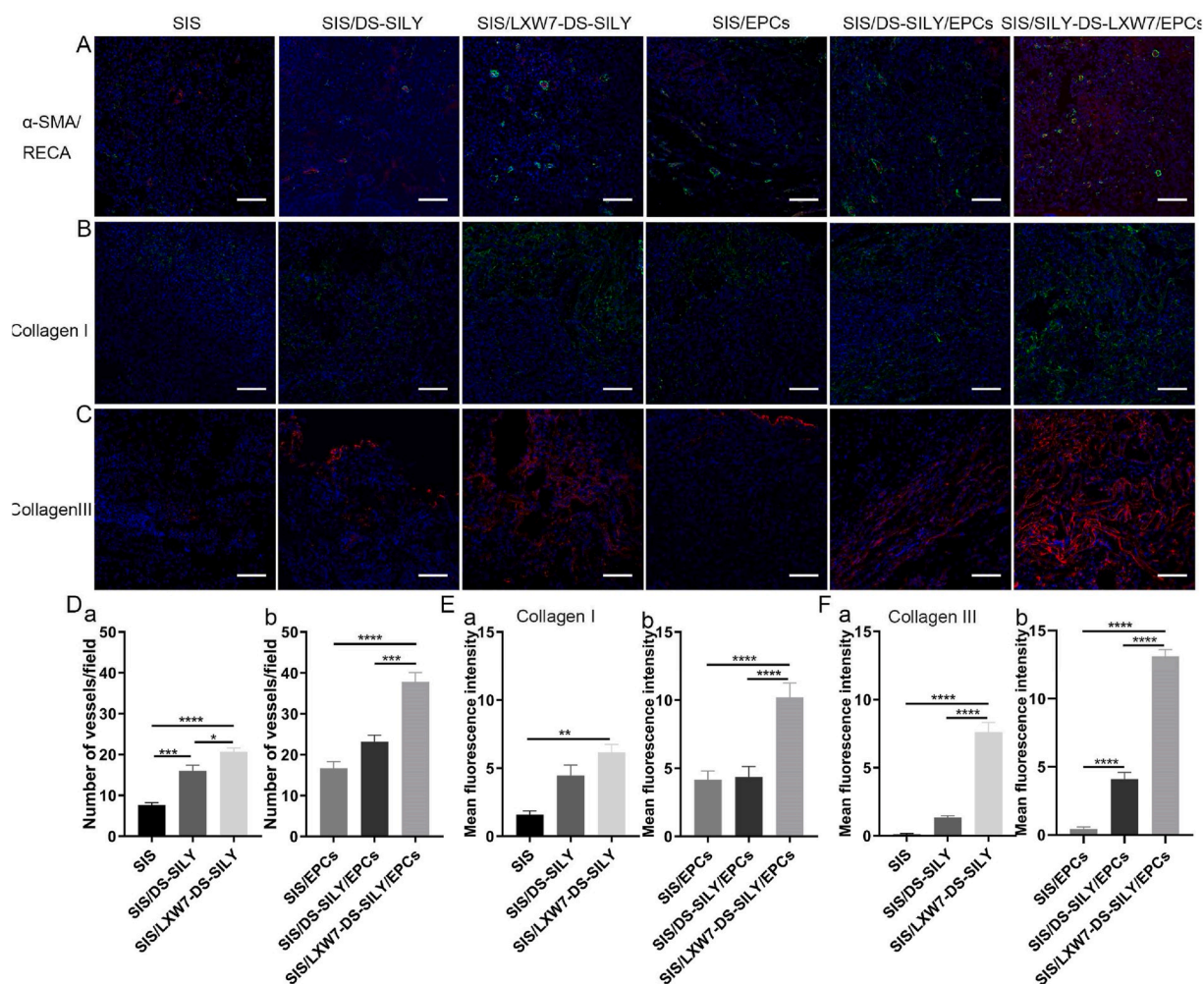
Fig. 9. Neovascularization and collagen deposition evaluation of wounds treated by different scaffolds under ischemic condition.
A. Blood vessels stained with α-SMA (green) and RECA (red) in wound bed at day 14 post surgery. **B–C.** Immunostaining of collagen I and collagen III expression in wound bed at day 14 post surgery. **D-F.** Quantification of the blood vessel number/field (D) and immunofluorescence intensity of collagen I (E) and collagen III (F). Data are expressed as mean ± SEM. ****p < 0.0001, ***p < 0.001, *p < 0.05, n = 3 per group. Scale bar = 100 μm.

wound closure and shorter wound lengths but showed no difference in the re-epithelialization process compared to SIS/DS-SILY/EPCs and the SIS/LXW7-DS-SILY groups. Under the ischemic condition, SIS/LXW7-DS-SILY/EPCs group again displayed a significantly faster rate of wound closure and shorter wound lengths, and in addition a rapid re-epithelialization compared to other groups. These results together suggest that LXW7 and EPCs improve the wound healing process.

We found the healing of the SIS/LXW7-DS-SILY/EPCs group is significantly better than the SIS/LXW7-DS-SILY group under the ischemic condition but showed no difference under the non-ischemic condition. SIS/LXW7-DS-SILY alone facilitated improved healing effect under the non-ischemic condition. From our previous studies, we have confirmed that LXW7 can effectively capture and support endogenous EPCs to bind to biomaterial-based scaffolds and formed functional endothelium *in vivo* [24]. Therefore, LXW7 conjugated to the SIS ECM scaffolds may promote wound healing by recruiting endogenous EPCs to the scaffolds at the wound sites when there is sufficient blood supply while other groups without LXW7 modification, e.g., SIS or SIS/DS-SILY groups, will not effectively capture and support endogenous EPCs to bind to the scaffolds. Vice versa, in highly ischemic diabetic wound areas, there is insufficient blood supply and therefore, endogenous EPCs are not abundantly available and will not be recruited as effectively to the wounds. That may explain why in ischemic conditions, the SIS/LXW7-DS-SILY group showed no difference compared to the SIS/DS-SILY group. Interestingly, once loaded with exogenous EPCs, even though the EPCs in the SIS/LXW7-DS-SILY/EPCs group were present in high numbers up to 24 h after transplantation and decreased

thereafter (Fig. 7D), the resulted increase in healing rate suggested that their presence for even a short period of time was sufficient to initiate tissue granulation, leading to functional re-epithelialization. As discussed above, the transplanted EPCs may be activated by LXW7 and the other environment cues and secrete biomolecules that support angiogenesis from the existing blood vessels. These secreted components, such as growth factors and extracellular vesicles may stay for a longer period of time even after the EPCs are gone which may display persistent effects in promoting tissue regeneration. In conclusion, our results suggest that LXW7 may aid in capture of the endogenous EPCs in the non-ischemic condition, and increase the survival and function of transplanted exogenous EPCs. The endogenous EPCs at the wound sites will also secrete paracrine factors that will stimulate the surrounding tissues and cells and thus promote angiogenesis and improve wound healing in both conditions [50].

When comparing the effects of SIS/DS-SILY under ischemic versus non-ischemic condition, we found that the healing of the SIS/DS-SILY group was as good as the SIS/LXW7-DS-SILY group (both were significantly better than the SIS group) under ischemic condition but showed no difference with the SIS group under non-ischemic condition. It is known that ischemic wounds induce excessive production and over-activity of MMPs in the wound environment, causing rapid degradation of new granulation tissue and countering the healing process [51–53]. DS-SILY was previously shown to improve collagen organization via inhibition of MMP-mediated collagen degradation [14]. The experimental results suggested that DS-SILY played a leading role in ischemic condition via protecting collagen from being degraded. In the non-ischemic condition however, collagen degradation may not be as significant which

may explain why the DS-SILY group showed no significant difference from the SIS group under non-ischemic condition (Fig. 4B panel a–b). Besides, no difference was found between the SIS and SIS/EPCs groups or the SIS/DS-SILY and SIS/DS-SILY/EPCs groups under ischemic condition (Fig. 7B panel d–e). Our results demonstrated that the ZDF rat ischemic skin flap model is an effective model to mimic the highly ischemic condition of DFU and thus can be used as a clinically relevant disease model for diabetic wound healing.

It is well known that wound neovascularization is essential in order to generate sufficient blood supply to the wound area for constant supply of oxygen and nutrition, the two important factors that promote healing [43]. The results obtained from the ischemic and non-ischemic wounds treated with the SIS/LXW7-DS-SILY/EPCs scaffolds showed an enhancement in angiogenesis when compared with other groups. Our previous study indicated that LXW7 can bind to EPCs and ECs via αvβ3 integrin and enhance EC biological functions by increasing phosphorylation of VEGF receptor 2 (VEGF-R2) and activating mitogen-activated protein kinase (MAPK) ERK1/2 [18]. Our *in vitro* data also showed that LXW7 and LXW7-DS-SILY modified surfaces promoted attachment and growth of ZDF-EPCs (Fig. 3). The results that SIS/LXW7-DS-SILY scaffolds alone had a positive effect on angiogenesis suggest that the LXW7 ligand potentially recruited and interacted with endogenous EPCs/ECs, and thus successfully promoted angiogenesis, neovascularization and wound healing in the diabetic wounds.

Proper collagen deposition and remodeling improve skin elasticity and toughness and greatly influence the outcomes of wound healing [54]. From immunohistological analyses (Fig. 9), we observed that all the modified scaffolds displayed abundant and relatively well-organized collagen fibers. Since in our previous studies, DS-SILY showed the ability to improve collagen organization [14], we expect that the modification with functional ligands DS-SILY or LXW7-DS-SILY may exert positive effects on the ECM molecules in the wound areas, such as limiting collagen degradation and maintaining the architecture of collagen fibers.

Collagen I and III are central components of the dermal ECM with collagen I constituting 80–85%, and collagen III constituting 8–11% of the dermal ECM, and both playing a vital role in wound healing [55]. Previous studies revealed that sufficient amounts of collagen III in the early wound healing process would accelerate healing and result in scarless skin [51]. DS-SILY can help with MMP mediated collagen degradation [14]. In this study, the DS-SILY and LXW7-DS-SILY ligand modified groups displayed a significantly higher intensity of collagen I or III deposition when compared to the control group, suggesting that the ligand may protect the matrix from MMP degradation, and thus suppress scar formation and mimic the wound healing process as in normal skin. Future studies will be needed to further assess this aspect of the wound healing induced with LXW7-DS-SILY.

In summary, this study demonstrates a novel therapeutic approach to accelerate diabetic ischemic wound healing by application of a functionalized combinatorial scaffold consisting of three functional components: 1) LXW7-DS-SILY, a bifunctional ligand; 2) SIS-ECM scaffold; and 3) EPCs. Further studies are necessary to explore matrix deposition at different time points, to investigate the cell populations recruited by the functionalized scaffolds, and to elucidate the potential mechanisms of LXW7 supporting the survival of transplanted EPCs, EPC paracrine signaling, and explore the potential application of this therapeutic approach to other diseases and conditions. Experiments involving large animals such as pigs which are more similar to human's skin structure and function to further validate the safety and efficacy of this therapeutic approach will be warranted before any clinical use.

5. Conclusions

This study has successfully demonstrated the importance of LXW7-DS-SILY functionalized SIS scaffolds in enhancing wound healing in a type 2 diabetic rat ischemic skin flap model. EPCs cultured on SIS/LXW7-DS-SILY scaffolds showed enhanced attachment and growth. In addition, the data indicated that wound closure, re-epithelialization, angiogenesis and collagen deposition were enhanced in the diabetic ischemic wounds treated with the SIS-ECM scaffold functionalized with LXW7-DS-SILY and EPCs. Thus, LXW7-

DS-SILY combined with an ECM scaffold and EPCs could be a promising novel treatment to accelerate healing of diabetic ischemic wounds, thereby reducing limb amputation and mortality rates of diabetic patients.

References

[1] International Diabetes Federation, IDF Diabetes Atlas, ninth ed., 2019. http://www.diabetesatlas.org.

[2] L.R. Kalan, J.S. Meisel, M.A. Loesche, J. Horwinski, I. Soaita, X. Chen, A. Uberoi, S. E. Gardner, E.A. Grice, Strain- and species-level variation in the microbiome of diabetic wounds is associated with clinical outcomes and therapeutic efficacy, Cell Host Microbe 25 (2019) 641–655, https://doi.org/10.1016/j.chom.2019.03.006, e5.

[3] A. Hingorani, G.M. Lamuraglia, P. Henke, M.H. Meissner, L. Loretz, K.M. Zinszer, V.R. Driver, R. Frykberg, T.L. Carman, W. Marston, J.L. Mills, M.H. Murad, The management of diabetic foot: a clinical practice guideline by the society for vascular surgery in collaboration with the American podiatric medical association and the society for vascular medicine, J. Vasc. Surg. 63 (2016) 3S–21S, https://doi.org/10.1016/j.jvs.2015.10.003.

[4] C. Wang, Q. Wang, W. Gao, Z. Zhang, Y. Lou, H. Jin, X. Chen, B. Lei, H. Xu, C. Mao, Highly efficient local delivery of endothelial progenitor cells significantly potentiates angiogenesis and full-thickness wound healing, Acta Biomater. 69 (2018) 156–169, https://doi.org/10.1016/j.actbio.2018.01.019.

[5] S. Kanji, H. Das, Advances of stem cell therapeutics in cutaneous wound healing and regeneration, Mediat. Inflamm. (2017), https://doi.org/10.1155/2017/5217967, 2017.

[6] A.C.D.O. Gonzalez, Z.D.A. Andrade, T.F. Costa, A.R.A.P. Medrado, Wound healing - a literature review, An. Bras. Dermatol. 91 (2016) 614–620, https://doi.org/10.1590/abd1806-4841.20164741.

[7] K. Kaushik, A. Das, Endothelial progenitor cell therapy for chronic wound tissue regeneration, Cytotherapy 21 (2019) 1137–1150, https://doi.org/10.1016/j.jcyt.2019.09.002.

[8] O.C. Velazquez, Angiogenesis and vasculogenesis: inducing the growth of new blood vessels and wound healing by stimulation of bone marrow-derived

progenitor cell mobilization and homing, J. Vasc. Surg. 45 (2007), https://doi.org/10.1016/j.jvs.2007.02.068. A39–A47.

[9] Z.J. Liu, O.C. Velazquez, Hyperoxia, endothelial progenitor cell mobilization, and diabetic wound healing, Antioxidants Redox Signal. 10 (2008) 1869–1882, https://doi.org/10.1089/ars.2008.2121.

[10] L. Wang, W. Wang, J. Liao, F. Wang, J. Jiang, C. Cao, S. Li, Novel bilayer wound dressing composed of SIS membrane with SIS cryogel enhanced wound healing process, Mater. Sci. Eng. C 85 (2018) 162–169, https://doi.org/10.1016/j.msec.2017.11.024.

[11] L. Lankford, Y.J. Chen, Z. Saenz, P. Kumar, C. Long, D. Farmer, A. Wang, Manufacture and preparation of human placenta-derived mesenchymal stromal cells for local tissue delivery, Cytotherapy 19 (2017) 680–688, https://doi.org/10.1016/j.jcyt.2017.03.003.

[12] P.S. Wolfe, S.A. Sell, G.L. Bowlin, Natural and synthetic scaffolds, Tissue Eng. (2011) 41–67, https://doi.org/10.1007/978-3-642-02824-3_3.

[13] P. Zhao, X. Li, Q. Fang, F. Wang, Q. Ao, X. Wang, X. Tian, H. Tong, S. Bai, J. Fan, Surface modification of small intestine submucosa in tissue engineering, Regen. Biomater. 7 (2020) 339–348, https://doi.org/10.1093/rb/rbaa014.

[14] K. Stuart, J. Paderi, P.W. Snyder, L. Freeman, A. Panitch, Collagen-binding peptidoglycans inhibit MMP mediated collagen degradation and reduce dermal scarring, 6, https://doi.org/10.1371/journal.pone.0022139, 2011.

[15] C.C. Reed, R.V. Iozzo, The role of decorin in collagen fibrillogenesis and skin homeostasis, Glycoconj. J. 19 (2002) 249–255, https://doi.org/10.1023/A:1025383913444.

[16] K.G. Vogel, J.A. Trotter, The effect of proteoglycans on the morphology of collagen fibrils formed in vitro, Top. Catal. 7 (1987) 105–114, https://doi.org/10.1016/S0174-173X(87)80002-X.

[17] P.G. Scott, C.M. Dodd, E.E. Tredget, A. Ghahary, F. Rahemtulla, Chemical characterization and quantification of proteoglycans in human post-burn hypertrophic and mature scars, Clin. Sci. 90 (1996) 417–425, https://doi.org/10.1042/cs0900417.

[18] D. Hao, W. Xiao, R. Liu, P. Kumar, Y. Li, P. Zhou, F. Guo, D.L. Farmer, K.S. Lam, F. Wang, A. Wang, Discovery and characterization of a potent and specific peptide ligand targeting endothelial progenitor cells and endothelial cells for tissue regeneration, ACS Chem. Biol. 12 (2017) 1075–1086, https://doi.org/10.1021/acschembio.7b00118.

[19] M.J. Webber, J. Tongers, C.J. Newcomb, K.T. Marquardt, J. Bauersachs, D. W. Losordo, S.I. Stupp, Erratum: supramolecular nanostructures that mimic VEGF as a strategy for ischemic tissue repair, Proc. Natl. Acad. Sci. Unit. States Am. 108 (33) (2011) 13438–13443, https://doi.org/10.1073/pnas.1016546108. Proc. Natl. Acad. Sci. U. S. A. 109 (2012) 9220.

[20] P.A. Walimbe T, T. Dehghani, A. Casella, J. Lin, A. Wang, A. Panitch, Proangiogenic collagen binding glycan therapeutic promotes endothelial cell Health: potential application for the treatment of ischemic wounds, ACS Biomater. Sci. Eng. (2021), https://doi.org/10.1021/acsbiomaterials.1c00336.

[21] J.E. Paderi, A. Panitch, Design of a synthetic collagen-binding peptidoglycan that modulates collagen fibrillogenesis, Biomacromolecules 9 (2008) 2562–2566, https://doi.org/10.1021/bm8006852.

[22] W. Xiao, Y. Wang, E.Y. Lau, J. Luo, N. Yao, C. Shi, L. Meza, H. Tseng, Y. Maeda, P. Kumaresan, R. Liu, F.C. Lightstone, Y. Takada, K.S. Lam, The use of one-bead one-compound combinatorial library technology to discover high-affinity αvβ3 integrin and cancer targeting arginine-glycine-aspartic acid ligands with a built-in handle, Mol. Canc. Therapeut. 9 (2010) 2714–2723, https://doi.org/10.1158/1535-7163.MCT-10-0308.

[23] A.N. Trujillo, S.L. Kesl, J. Sherwood, M. Wu, L.J. Gould, Demonstration of the rat ischemic skin wound model, J. Vis. Exp. 2015 (2015) 1–7, https://doi.org/10.3791/52637.

[24] D. Hao, F. Fan, W. Xiao, R. Liu, C. Pivetti, T. Walimbe, F. Guo, X. Zhang, D. L. Farmer, F. Wang, A. Panitch, K.S. Lam, A. Wang, Rapid endothelialization of small diameter vascular grafts by a bioactive integrin-binding ligand specifically targeting endothelial progenitor cells and endothelial cells, Acta Biomater. 108 (2020) 178–193, https://doi.org/10.1016/j.actbio.2020.03.005.

[25] S. Guo, L.A. DiPietro, Critical review in oral biology & medicine: factors affecting wound healing, J. Dent. Res. 89 (2010) 219–229, https://doi.org/10.1177/0022034509359125.

[26] D. Lou, Y. Luo, Q. Pang, W.Q. Tan, L. Ma, Gene-activated dermal equivalents to accelerate healing of diabetic chronic wounds by regulating inflammation and promoting angiogenesis, Bioact. Mater. 5 (2020) 667–679, https://doi.org/10.1016/j.bioactmat.2020.04.018.

[27] Q. Tan, Y. Li, X. Li, S. Zhang, Hyperinsulinemia impairs functions of circulating endothelial progenitor cells, Acta Diabetol. 56 (2019) 785–795, https://doi.org/10.1007/s00592-019-01314-9.

[28] H. Wang, P. Agarwal, Y. Xiao, H. Peng, S. Zhao, X. Liu, S. Zhou, J. Li, Z. Liu, X. He, A nano-in-micro system for enhanced stem cell therapy of ischemic diseases. https://doi.org/10.1021/acscentsci.7b00213, 2017.

[29] K. Li, D. Keun, K. Park, S. Song, J. Yeon, J. Kim, H. Yun, S. Won, C. Roh, E. Jeon, D. Kim, W. Suh, Biomaterials Enhanced dermal wound neovascularization by targeted delivery of endothelial progenitor cells using an RGD- g -PLLA scaffold, Biomaterials 30 (2009) 3742–3748, https://doi.org/10.1016/j.biomaterials.2009.03.053.

[30] M. Noh, Y.H. Choi, Y. An, D. Tahk, S. Cho, Magnetic nanoparticle-embedded hydrogel sheet. https://doi.org/10.1021/acsbiomaterials.8b01307, 2019.

[31] J. Ho, C. Walsh, D. Yue, A. Dardik, U. Cheema, Current advancements and strategies in tissue engineering for wound healing: a comprehensive review, Adv. Wound Care 6 (2017) 191–209, https://doi.org/10.1089/wound.2016.0723.

[32] M. Pittenger, Sleuthing the source of regeneration by MSCs, Stem Cell. 5 (2009) 8–10, https://doi.org/10.1016/j.stem.2009.06.013.

[33] A.I. Caplan, D. Correa, Perspective the MSC : an injury drugstore, Stem Cell. 9 (2011) 11–15, https://doi.org/10.1016/j.stem.2011.06.008.

[34] A. Wang, E.G. Brown, L. Lankford, B.A. Keller, C.D. Pivetti, N.A. Sitkin, M. S. Beattie, J.C. Bresnahan, Placental mesenchymal stromal cells rescue ambulation in ovine myelomeningocele, Stem Cells Transl Med 2 (2015) 659–669, https://doi.org/10.5966/sctm.2014-0296.

[35] P.D. Robbins, A.E. Morelli, Regulation of immune responses by extracellular vesicles, Nat. Publ. Gr. 14 (2014) 195–208, https://doi.org/10.1038/nri3622.

[36] P. Kumar, J.C. Becker, K. Gao, R.P. Carney, L. Lankford, B.A. Keller, K. Herout, K. S. Lam, D.L. Farmer, A. Wang, Neuroprotective effect of placenta-derived mesenchymal stromal cells : role of exosomes, 1–14, https://doi.org/10.1096/fj.201800972R, 2019.

[37] J. Phan, A. Wang, Engineering mesenchymal stem cells to improve their exosome efficacy and yield for cell-free therapy, J. Extracell. Vesicles 7 (2018), https://doi.org/10.1080/20013078.2018.1522236.

[38] R.M. Amorim, K.C. Clark, N.J. Walker, P. Kumar, K. Herout, D.L. Borjesson, A. Wang, Placenta-derived multipotent mesenchymal stromal cells : a promising potential cell- based therapy for canine inflammatory brain disease, 1–12, https://doi.org/10.1186/s13287-020-01799-0, 2020.

[39] K. Gao, P. Kumar, E. Cortez-Toledo, D. Hao, L. Reynaga, M. Rose, C. Wang, D. Farmer, J. Nolta, J. Zhou, P. Zhou, A. Wang, Potential long-term treatment of hemophilia A by neonatal co-transplantation of cord blood-derived endothelial colony-forming cells and placental mesenchymal stromal cells, Stem Cell Res. Ther. 10 (2019) 1–15, https://doi.org/10.1186/s13287-019-1138-8.

[40] K. Gao, S. He, P. Kumar, D. Farmer, J. Zhou, A. Wang, Clonal isolation of endothelial colony-forming cells from early gestation chorionic villi of human placenta for fetal tissue regeneration, World J. Stem Cell. (2020) 123–138, https://doi.org/10.4252/wjsc.v12.i2.123.

[41] M. Rose, K. Gao, E. Cortez-toledo, E. Agu, A.A. Hyllen, K. Conroy, A. Wang, P. Zhou, J.A. Nolta, Endothelial cells derived from patients ' induced pluripotent stem cells for sustained factor VIII delivery and the treatment of hemophilia A, 686–696, https://doi.org/10.1002/sctm.19-0261, 2020.

[42] S. Balaji, T.M. Crombleholme, A. King, The role of endothelial progenitor cells in postnatal Vasculogenesis : implications for therapeutic neovascularization and wound, Healing 2 (2013) 283–295, https://doi.org/10.1089/wound.2012.0398.

[43] Y. Kato, T. Iwata, S. Morikawa, M. Yamato, T. Okano, Y. Uchigata, Allogeneic transplantation of an adipose-derived stem cell sheet combined with artificial skin accelerates wound healing in a rat wound model of type 2 diabetes and obesity, Diabetes 64 (2015) 2723–2734, https://doi.org/10.2337/db14-1133.

[44] N. Goonoo, A. Bhaw-Luximon, Analyzing polymeric nanofibrous scaffold performances in diabetic animal models for translational chronic wound healing research, Nanotechnol. Rev. 6 (2017) 583–600, https://doi.org/10.1515/ntrev-2017-0162.

[45] P.N. Chander, O. Gealekman, S.V. Brodsky, S. Elitok, A. Tojo, M. Crabtree, S. S. Gross, M.S. Goligorsky, Nephropathy in Zucker diabetic fat rat is associated with oxidative and nitrosative stress: prevention by chronic therapy with a peroxynitrite scavenger ebselen, J. Am. Soc. Nephrol. 15 (2004) 2391–2403, https://doi.org/10.1097/01.ASN.0000135971.88164.2C.

[46] R. Slavkovsky, R. Kohlerova, V. Tkacova, A. Jiroutova, B. Tahmazoglu, V. Velebny, M. Rezačová, L. Sobotka, J. Kanta, Zucker diabetic fatty rat: a new model of impaired cutaneous wound repair with type II diabetes mellitus and obesity, Wound Repair Regen. 19 (2011) 515–525, https://doi.org/10.1111/j.1524-475X.2011.00703.x.

[47] L.J. Coppey, J.S. Gellett, E.P. Davidson, J.A. Dunlap, M.A. Yorek, Changes in endoneurial blood flow, motor nerve conduction velocity and vascular relaxation of epineurial arterioles of the sciatic nerve in ZDF-obese diabetic rats, Diabetes. Metab. Res. Rev. 18 (2002) 49–56, https://doi.org/10.1002/dmrr.257.

[48] C.L. Oltman, L.J. Coppey, J.S. Gellett, E.P. Davidson, D.D. Lund, M.A. Yorek, Progression of vascular and neural dysfunction in sciatic nerves of Zucker diabetic fatty and Zucker rats, Am. J. Physiol. Endocrinol. Metab. 289 (2005) 113–123, https://doi.org/10.1152/ajpendo.00594.2004.

[49] P.B. Milan, N. Lotfibakhshaiesh, M.T. Joghataie, J. Ai, A. Pazouki, D.L. Kaplan, S. Kargozar, N. Amini, M.R. Hamblin, M. Mozafari, A. Samadikuchaksaraei, Accelerated wound healing in a diabetic rat model using decellularized dermal matrix and human umbilical cord perivascular cells, Acta Biomater. 45 (2016) 234–246, https://doi.org/10.1016/j.actbio.2016.08.053.

[50] S. Xu, J. Zhu, L. Yu, G. Fu, Endothelial progenitor Cells : current development of their paracrine therapy in cardiovascular therapy, 59, https://doi:10.1097/FJC.0b013e3182440338, 2012, 387–396.

[51] C. Wang, M. Wang, T. Xu, X. Zhang, C. Lin, W. Gao, H. Xu, B. Lei, C. Mao, Engineering bioactive self-healing antibacterial exosomes hydrogel for promoting chronic diabetic wound healing and complete skin regeneration, Theranostics 9 (2019) 65–76, https://doi.org/10.7150/thno.29766.

[52] P. Yang, Q. Pei, T. Yu, Q. Chang, D. Wang, M. Gao, X. Zhang, Y. Liu, Compromised wound healing in ischemic type 2 diabetic rats, PloS One 11 (2016) 1–19, https://doi.org/10.1371/journal.pone.0152068.

[53] S. Eming, H. Smola, B. Hartmann, G. Malchau, R. Wegner, T. Krieg, S. Smola-hess, Biomaterials the inhibition of matrix metalloproteinase activity in chronic wounds by a polyacrylate, superabsorber 29 (2008) 2932–2940, https://doi.org/10.1016/j.biomaterials.2008.03.029.

[54] J. Chi, X. Zhang, C. Chen, C. Shao, Y. Zhao, Y. Wang, Antibacterial and angiogenic chitosan microneedle array patch for promoting wound healing, Bioact. Mater. 5 (2020) 253–259, https://doi.org/10.1016/j.bioactmat.2020.02.004.

[55] E. Davison-kotler, W.S. Marshall, E. Garc, Sources of collagen for biomaterials in skin wound healing, 1–15, https://doi.org/10.3390/bioengineering6030056, 2019.